Meiosis-specific genes play roles in ploidy reduction in *Cryptococcus neoformans* titan cells

Zhuyun Bian[1], Kayla Wilhoit[2], Julian Liber[2], Anushka Peer[1], Ziyan Xu[1], Paul Magwene[1], Sheng Sun[1], and Joseph Heitman[1]*

[1] Department of Molecular Genetics and Microbiology, Duke University Medical Center, Durham, North Carolina, USA

[2] Department of Biology, Duke University, Durham, North Carolina, USA

*Corresponding author:

Joseph Heitman (heitm001@duke.edu)

Key Words

Fungi, titan cell, ploidy reduction, Dmc1, Spo11

ABSTRACT

Cryptococcus neoformans is a fungal pathogen of humans that causes life-threatening meningoencephalitis. During infection, enlarged, polyploid titan cells are produced that promote survival, evade immune cells, and generate diverse progeny. These titan cells divide to produce haploid, aneuploid or diploid daughter cells with enhanced stress tolerance; however, how ploidy reduction occurs is poorly understood. Here, we show that titan cells developed from diploid strains predominantly produce diploid daughter cells with haploid daughters observed infrequently. We further demonstrate that meiosis-specific genes, including *DMC1* and *SPO11*, are critical for stable inheritance of a diploid genome in the daughter cells. Specifically, deletion of these genes in a heterozygous diploid background results in: 1) titan cells with a significantly reduced capacity to produce daughter cells; 2) increased phenotypic variation among daughter cells produced by the titan cells, including traits that could be relevant to cell growth and viability; and 3) daughter cells produced by the titan cells exhibiting high levels of loss of heterozygosity (LOH) and aneuploidy, suggested elevated genome instability. Taken together, these findings demonstrate the importance of meiosis-specific genes in the ploidy reduction process of titan cells derived from a heterozygous diploid background in an important human fungal pathogen.

SIGNIFICANCE

Polyploid titan cells are central to *Cryptococcus neoformans* persistence during infection, yet how they reduce ploidy to generate daughter cells was unclear. We show that the meiosis-specific factors Dmc1 and Spo11 are critical for titan cells to produce viable daughter cells specifically in a heterozygous diploid context, ensuring chromosome stability without introducing detectable canonical meiotic recombination. Loss of either gene compromises daughter cell production and causes genome instability (LOH, aneuploidy) and phenotypic heterogeneity. These findings reveal a “para-meiosis” safeguard that preserves genome balance during titan cell depolyploidization in *C. neoformans*.

INTRODUCTION

Cryptococcus neoformans is a globally distributed pathogen that causes meningoencephalitis predominantly in immunocompromised hosts, most notably people living with HIV/AIDS or immunosuppressed for organ transplant or during cancer chemotherapy (1, 2). A recent study revealed that cryptococcal disease causes ~112,000 deaths and accounts for ~19% of AIDS-related mortality worldwide each year, underscoring its disproportionate impact on advanced HIV disease (3). During infection, *C. neoformans* undergoes marked morphogenetic transitions including the production of titan cells and seed cells (4-9). While seed cells are small cells (~5 µm in diameter) that facilitate dissemination to extrapulmonary organs, titan cells are enlarged cells (>10 µm) that contribute to persistence and virulence of *Cryptococcus* in part through their size and altered surface properties that inhibit phagocytosis (10-12). As defined by earlier studies, titan cells are an inducible, host-associated morphotype characterized by extreme cell enlargement (diameter greater than 10 µm), thickened cell wall and capsule, and polyploidy (7, 13-17). In addition to their inhibitory activity against phagocytes, polyploid titan cells can bud off smaller haploid, aneuploid, or diploid daughter cells that display heightened resistance to diverse stresses (18, 19). However, the mechanisms and regulation of this ploidy reduction process remain poorly understood.

Sexual reproduction in *C. neoformans* can proceed via different cycles including **a** × α heterothallic sexual reproduction, unisexual reproduction, and pseudosexual reproduction (20-24). All three modes of sexual reproduction involve regulated ploidy transitions and a terminal meiotic ploidy reduction. In both **a** × α sexual and unisexual reproduction, haploid cells undergo plasmogamy and form dikaryotic hyphae, and the nuclei then fuse (karyogamy) within the basidium to generate a transient diploid nucleus that undergoes meiosis. During meiosis, programmed meiotic recombination shuffles alleles between parental homologs. Spo11 initiates this process by generating DNA double-strand breaks (DSBs), and the recombinase Dmc1 promotes a homology search and strand invasion to repair these DSBs and produce meiotic recombination (25, 26). The *DMC1* and *SPO11* genes are both meiosis-specific and highly conserved from yeasts to humans. Proper homolog pairing and crossover formation ensure accurate reductional segregation, thereby achieving ploidy reduction and producing haploid basidiospores with genetic variation (27, 28).

In addition to the facts that meiosis involves a ploidy reduction process and meiosis-specific genes have also been observed to be upregulated or activated during ploidy reduction processes across diverse systems, whether and how these factors functionally drive depolyploidization has remained unclear. In human cancer models, polyploid cells generated after genotoxic stress or mitotic catastrophe up-regulate canonical meiotic components (e.g., *DMC1*, *REC8*, *SYCP* proteins, *SPO11*) as they revert to smaller, proliferative progeny, linking a "pro-meiotic" transcriptional state to depolyploidization (29). In a Notch-induced Drosophila tumor model, tumor growth relies on cycles of polyploidization and reduction, and comparative RNA-seq analyses show that DNA-damage response genes with meiotic roles are up-regulated and required for the ploidy-reduction division (30). Analogously, the human fungal pathogen *Candida albicans* undergoes a parasexual cycle in which diploid cells fuse to form tetraploids and then return toward diploidy via concerted (largely random) chromosome loss, rather than meiosis. This depolyploidization and homologous recombination require meiosis-toolkit proteins such as Spo11 and Rec8 (31, 32).

In *C. neoformans*, meiotic genes were shown to be transiently expressed during infection, and deletion of meiotic genes increases the proportion of large cells during infection and delays the ploidy reduction of these cells (19). However, it is not yet clear whether the depolyploidization of *C. neoformans* titan cells is a meiotic or meiotic-like process. In this study, we utilized a heterozygous diploid strain to carry out a detailed analysis of genome dynamics and transitions during the depolyploidization of *C. neoformans* titan cells. We show that the meiosis-specific genes *DMC1* and *SPO11* are required for efficient production of viable daughter cells from polyploid titan cells containing genome-wide heterozygosity, establishing a direct, genetics-based link between meiosis factors and titan-cell ploidy reduction. Loss of the meiosis-specific genes *DMC1* or *SPO11* lead to the production of titan daughter cells with significantly increased phenotypic and genotypic heterogeneity, associated with rampant genomic instability during ploidy reduction, including LOH and aneuploidy that were often associated with reduced colony size and possibly inviability. Despite the observed dependency or meiosis-specific genes, we detected no canonical meiotic recombination in daughter cells derived from the titan cells formed by the wild-type heterozygous diploid strains. Thus, our findings indicate that titan cell depolyploidization co-opts meiotic proteins not to drive crossover formation, but instead to

stabilize chromosome segregation, thereby safeguarding genome integrity during this ploidy reduction program in *C. neoformans*.

RESULTS

Meiosis-specific genes *DMC1* and *SPO11* are required for ploidy reduction when heterozygous diploid titan cells produce daughter cells

In this study, we induced *C. neoformans* cells to form titan cells and isolated titan cells through micro-dissection for analysis. Because titan cells were dissected based on size, usually defined as >10 μm, it was essential to confirm that our size-based isolation approach enriches for polyploid titan cells rather than enlarged haploid or diploid cells that might be arrested in G1 phase. To achieve this, we first grew the diploid strain CnLC6683 (33) under titan cell inducing conditions, then filtered the cell culture through a 10 μm filter to collect enlarged cells. Cell diameter measurements revealed a clear shift in size distribution toward large cells, with the proportion of large cells (>10 μm) increasing from ~12% in the unfiltered cell culture to ~65% post-filtration (Figure 1A). We next accessed DNA content of both pre- and post-filtration cell cultures through propidium-iodide staining and flow cytometry. We observed a clear enrichment of cells with elevated DNA content (>4C) in the filtered cultures (~43%) than the pre-filtration cultures (~11%) (Figure 1A). Together, these data confirm that size-based isolation effectively enriches for polyploid titan cells, therefore ensuring that subsequent analyses reflect *bona fide* titan cell biology.

The central question of this study was whether the mechanism by which polypoid titan cells produce haploid or aneuploid daughter cells resembled a meiotic process. Because meiotic recombination, a hallmark of meiosis, can only be tracked when homologous chromosomes carry distinguishable sequences, we constructed a heterozygous diploid strain BH by fusing the genetically distinct haploid strains Bt63**a** and H99α. While H99α belongs to the *C. neoformans* lineage VNI, Bt63**a** is a natural isolate that belongs to the lineage VNBI and exhibits ~0.5% genetic divergence and one chromosomal translocation from H99α (20, 34). Previous studies on titan cells in *C. neoformans* mainly analyzed haploid strains and it has been reported that haploid-derived titan cells can produce haploid, aneuploid, or diploid daughter cells (7, 14, 18). To investigate these features in a diploid cell background, the BH strain was employed for titan cell induction. We micro-dissected individual titan cells and allowed them to grow on YPD agar

media at 30˚C for 48 hours. Colonies (titan colony cells) that formed on YPD agar media were then picked and analyzed by flow cytometry. Interestingly, a majority of the titan colony cells exhibited a diploid DNA content with only 2.5% being haploid cells (2 out of 80) (Figure 1B). In contrast, when the haploid strain H99α was induced to form titan cells and then micro-dissected, all of the titan colony cells had a haploid DNA content (60 out of 60) (Figure 1B). Our data suggest that the ploidy levels of the cells produced by the titan cells correspond to those of the progenitor cells. We next investigated whether the meiosis-specific genes *DMC1* and *SPO11* are involved in the ploidy reduction processes when titan cells are forming colonies.

To this end, we first constructed a BH *dmc1*Δ/*dmc1*Δ homozygous deletion mutant by fusing two haploid *dmc1* deletion mutants (H99α *dmc1*Δ and Bt63**a** *dmc1*Δ). Similarly, we also generated a homozygous deletion mutant BH *spo11*Δ/*spo11*Δ. The two mutant strains, together with the BH wild-type strain, were analyzed for induction of titan cells, which were then micro-dissected onto YPD agar media, and allowed to form colonies. We found that while approximately 70% of dissected titan cells formed by the BH wild-type strain gave rise to viable colonies (Figure 1C), the proportion of titan cells that formed viable colonies was significantly reduced in both the BH *dmc1*Δ/*dmc1*Δ (~10%) and the BH *spo11*Δ/*spo11*Δ (~40%) mutant strains (Figure 1C). We also micro-dissected normal sized yeast cells from the same cell cultures that were used for titan cell dissection, and all three genotypes displayed comparable colony-forming efficiencies of ~90%, indicating that deletion of *DMC1* or *SPO11* does not compromise general cell viability under titan cell inducing conditions.

To determine whether the requirement for *DMC1* and *SPO11* during depolyploidization is specific to a diploid context, we then assessed the colony-forming efficiency in haploid strains. Specifically, we induced and micro-dissected titan cells from the haploid wild-type strain H99α and its two mutants H99α *dmc1*Δ and H99α *spo11*Δ. Titan cells dissected from all three genotypes formed colonies at 100% efficiency, similar to those by the yeast-like cells dissected from the same cultures (>90%) (Figure 1D). This indicates that not only deletion of the *DMC1* and *SPO11* genes has no general growth defect, but also that they are not required for the colony-forming ability of titan cells produced from haploid progenitor cells.

Because the BH strains are heterozygous diploids, we next assessed whether the requirement for Dmc1 and Spo11 the colony formation by titan cells produced by these strains are related to the heterozygosity present in their genomes. To this end, we conducted similar titan

cell induction and dissection analyses with CnLC6683, a wild-type homozygous diploid strain, as well as *dmc1*Δ/*dmc1*Δ and *spo11*Δ/*spo11*Δ deletion mutants in the CnLC6683 background. In this case, we observed similarly high colony forming efficiency for all three genotypes in both titan cells (~60%) and yeast-like cells (~90%) (Figure 1E), suggesting the deletion of *DMC1* and *SPO11* does not have a significant effect on the titan cell colony forming ability in a homozygous diploid genetic background.

Taken together, these results demonstrate that the two meiosis-specific genes, *DMC1* and *SPO11*, are essential for the depolyploidization of titan cells produced by diploid cells when there is genome-wide heterozygosity, but they are dispensable if the progenitor strains are either haploid or homozygous diploid.

Deletion of meiosis-specific genes leads to elevated phenotypic heterogeneity among cells produce by titan cells with genome-wide heterozygosity

Given the critical roles of *DMC1* and *SPO11* during the process of ploidy reduction and their canonical function in meiotic recombination that generates offspring diversity, we next investigated whether phenotypic variation is present among cells produced by the dissected titan cells. For this, we first performed carbon source utilization assays with Biolog YT microplates for three titan colony cells and their corresponding progenitor strains in each of the three genotypic backgrounds (BH wild-type, BH *dmc1*Δ/*dmc1*Δ, and BH *spo11*Δ/*spo11*Δ). This pilot screen not only revealed considerable variation in carbon source utilization among the cells produced from titan cells, but also allowed us to identify a subset of carbon sources that exhibited the most significant phenotypic variation among these cells, from which we chose D-ribose, L-arabinose, maltose, and sucrose for further single-carbon assays with an expanded set of titan colony cells (Supplemental Figure S1).

Interestingly, for each of the four carbon sources tested, cells produced by the BH *dmc1*Δ/*dmc1*Δ and BH *spo11*Δ/*spo11*Δ titan cells consistently showed significantly higher phenotypic variation, manifested as wider spread of the phenotypic values than those produced by their corresponding BH wild-type strains, indicating greater heterogeneity in carbon source utilization among cells produced by BH mutant titan cells (Figure 2A and Supplemental Figure S2A, Levene's test). In contrast, when the same assays were performed for the cells produced by titan cells formed by CnLC6683 wild-type, CnLC6683 *dmc1*Δ/*dmc1*Δ, and CnLC6683

*spo11*Δ/*spo11*Δ strains, we observed no obvious difference in the levels of phenotypic variation among cells in the different genetic backgrounds (Figure 2B and Supplemental Figure S2B, Levene's test). Together, these results show that when heterozygosity is present in the genome, the absence of Dmc1 or Spo11 leads to titan cells producing daughter cells with significantly increased phenotypic variation.

Deletion of the meiosis-specific genes leads to increased genome instability during depolyploidization of titan cells with genome-wide heterozygosity

Given the increased phenotypic variation in carbon-source utilization observed among cells produced by the BH *dmc1*Δ/*dmc1*Δ and BH *spo11*Δ/*spo11*Δ titan cells, we hypothesized that these phenotypic changes might be associated with underlying genomic changes that occurred during titan cell depolyploidization. To test this, we conducted whole-genome sequencing of colonies formed by titan cells derived from BH wild-type (9 colonies), BH *dmc1*Δ/*dmc1*Δ (12 colonies) and BH *spo11*Δ/*spo11*Δ (37 colonies), and mapped the reads to both the H99 and the Bt63 reference genomes. Our analyses revealed six different types of large scale genetic changes. Five of them (types 1-5) involve various types of loss of heterozygosity (LOH) through segmental or whole-chromosome deletion/duplication, as well as aneuploidy, and type 6 represents cases where haploid cells were produced from the titan cells (Figure 3A and Supplemental Figure S3). Notably, we found more cases with whole-chromosome alterations than those that only involved segmental chromosomal changes (Figure 3B).

When comparing among cells produced from different genetic backgrounds, a vast majority of those produced by the BH wild-type titan cells (78%) retained an unaltered genome, with only 22% containing genomic changes that belong to the six types characterized above (Figure 3C). In contrast, 57% of cells derived from the BH *spo11*Δ/*spo11*Δ titan cells and 67% of the cells derived from the BH *dmc1*Δ/*dmc1*Δ titan cells harbored various genomic alterations (Figure 3C), indicating that loss of *DMC1* or *SPO11* markedly increases the genomic instability and compromises the depolyploidization process in mutant titan cells. Interestingly, micro-dissected titan cells from both wild-type and mutant backgrounds formed colonies of varying sizes on YPD solid plates, and our analyses showed that every small-sized colony contained genomic alterations of various types (Figure 3D), suggesting that such chromosomal changes

likely compromise cell growth, and that titan cells incapable of forming colonies may harbor even more extensive genomic disruptions that prevent daughter cell production.

Taken together, we indeed detected increased levels of genomic alteration in cells produced by the BH *dmc1*Δ/*dmc1*Δ and BH *spo11*Δ/*spo11*Δ mutant titan cells, which is consistent with the observed increase in their phenotypic variation.

No canonical meiotic recombination or crossovers were observed in BH titan daughter cells

Our phenotypic and genotypic analyses demonstrated that the meiosis-specific genes *DMC1* and *SPO11* are critical for faithful depolyploidization process of heterozygous titan cells to produce viable daughter cells and form colonies. It is known that Spo11 and Dmc1 function prominently during meiosis by introducing and repairing double-strand breaks, respectively, contributing to the formation of crossovers and proper segregation of homologous chromosomes. We hypothesized that these two proteins might play similar roles during titan cell depolyploidization. To investigate this, we sought to analyze the cells produced from the BH wild-type titan cells to see if there were any signs of crossing over in their genomes.

Our hypothesis is that meiosis and crossovers occur when daughter cells are produced from titan cells; thus, the population of cells within the colony formed by a titan cell could be heterogenous in their genomic compositions, complicating the detection of meiotic crossovers. Instead, we first dissected titan cells formed by the BH wild-type strain onto YPD. Next, for each dissected titan cell, we separated and transferred every daughter cell that directly budded off the titan cell onto a different location (i.e. primary daughter cells), as well as cells that budded off these primary daughter cells (i.e. secondary daughter cells) within a 12-hour window (Figure 4A and Supplemental Figure S4). In total, we dissected 12 titan cells. Three of them did not produce any daughter cell, and corresponds to a colony forming efficiency of 75%, which is comparable to our earlier observations of colony forming efficiency for the BH wild-type titan cell. Among the nine titan cells that produced daughter cells, we observed considerable variation in their ability to produce daughter cells: five titan cells produced at least four primary daughter cells, one titan cell produced three primary daughter cells, two titan cells produced two primary daughters, and one titan cell only produced a single primary daughter cell during the 12-hour window (Figure 4A and Supplemental Figure S4). In addition, primary daughter cells were

observed to be produced simultaneously in four titan cells and were marked as Bd1 and Bd2 (Figure 4A and Supplemental Figure S4).

We first subjected all of the dissected cells to Illumina whole genome sequencing. Except for the cells in group 6, all other cells exhibited a euploid 2N karyotype, carrying one H99-derived homolog and one Bt63-derived homolog for each chromosome. Loss of heterozygosity (LOH) on chromosome 9 (only the Bt63**a** allele) and on Chromosome 12 (only the H99α allele) was observed in all samples in group 6 (Figure 4B). Furthermore, the secondary daughter cell Ba-a harbors an additional copy of the H99α-derived chromosome 7, which likely arose during vegetative growth. Interestingly, all four samples in group 6 formed small colonies compared to the wild type BH (Supplemental Figure S4), suggesting that the identified LOH events may confer a growth disadvantage.

Because there is only ~0.5% genetic divergence between the two parental genomes, Bt63 and H99, which constitute the diploid genome of the BH wild-type strain, the level of polymorphism may not be sufficient for detection of crossovers using the short reads generated from Illumina whole genome sequencing. To overcome this, we conducted Nanopore long-read sequencing for two primary daughter cells produced by titan cell No. 1, and one primary daughter cell from each of the other eight titan cells. We developed an analysis pipeline that is able to detect sequence breakpoints, which are junctions within the Nanopore reads where sequences on the two sides of the junction are of different origin (i.e. Bt63 and H99), indicative of crossovers (Figure 4C), and validated the pipeline with a simulated dataset that contains crossovers (Figure 4D and Supplemental Figure S5).

We next analyzed the Nanopore long-reads generated from the 10 primary daughter cells. To our surprise, we did not detect any statistically significant signal of crossover in any of the daughter cells. Specifically, the Nanopore reads all showed profiles that are distinct from the simulated dataset with crossovers, and resembled the simulated dataset without recombination. The plot generated for Chromosome 14 is shown as an example (Figure 4D). Further inspection of the reads underlying the minor breakpoint candidates confirmed that they are not crossovers and all of them are located within genomic regions with highly repetitive sequences or transposable elements (e.g. centromeric and telomeric regions). Thus, while Dmc1 and Spo11 are important for faithful depolyploidization of titan cells with genome-wide heterozygosity, our analyses of daughter cells produced by the titan cells showed that they have no canonical meiotic

crossovers in their genomes, indicating that the two meiosis-specific genes might be exerting their influence on titan cell depolyploidization through novel mechanisms yet to be characterized.

DISCUSSION

In this study, our data revealed a severe, heterozygosity-dependent defect in ploidy reduction of titan cells when the meiosis-specific genes *DMC1* or *SPO11* were deleted. The percentage of titan cells that produced viable daughter cells decreased significantly, and the surviving titan cell colonies frequently carried LOH or aneuploidy that was often linked to smaller colony size. The reason why these segregation errors are uniquely deleterious in a heterozygous genome could be that LOH converts heterozygous loci with divergent Bt63/H99 alleles to homozygosity, therefore unmasking recessive defects and/or disrupting favorable allele combinations of co-evolved genes, and aneuploidy distorts allelic dosage compared to the original euploid genome. In contrast, while Dmc1 and Spo11 may still participate in ploidy reduction of titan cells produced by haploid or homozygous diploid strains, the phenotypic consequences of their absence could be attenuated because: 1) without heterozygosity, genomes with the reciprocal crossovers and whole chromosome LOH observed in the BH backgrounds are both effectively dosage-balanced diploids resembling that of the wild-type progenitor strain; and 2) in cases of aneuploidy, gene expression imbalance would be less disruptive when both homologs are identical. Indeed, Dmc1 has been shown previously to be activated during infection of the host, when titan cell formation is induced (29). It should be noted that the H99 genome exhibits one reciprocal chromosomal translocation compared to Bt63, which can further sensitize the system in strains of the BH background as LOH or aneuploidy affecting these chromosomes can cause severe local copy number or structure imbalances, amplifying fitness costs and explaining the strong dependency on *DMC1* and *SPO11* to stabilize chromosome transmission during titan cell depolyploidization.

Because *DMC1* and *SPO11* are involved in the ploidy reduction process when titan cells produce daughter cells, and the canonical function of these two meiosis-specific genes is to generate (Spo11) and repair (Dmc1) DNA DSBs, which will result in crossover events, we hypothesized that cross-over events might exist in the titan daughter cells derived from the heterozygous diploid BH strain. Interestingly, we found no evidence of canonical crossovers between Bt63 and H99 homologs with apparent breakpoint enrichments all localized to telomeric,

centromeric, or repetitive regions. Importantly, however, the absence of a Bt63/H99 crossover signal does not exclude recombination during the ploidy reduction process. Polyploid titan cells can harbor multiple copies of the same parental homolog, and recombination that occurs between genetically identical templates, for example, two Bt63 copies or two H99 copies, would be undetectable with SNP-based analysis, because recombination would have occurred between identical sequences. Likewise, non-crossover repair such as Synthesis-dependent strand-annealing (SDSA) (35, 36) or very short gene-conversion tracts (37) could fall below our detection thresholds, particularly in regions of low marker density. Thus, our data argue against frequent or widespread genetic exchange between divergent homologs during titan cell depolyploidization, but they remain compatible with recombination on identical templates, a route that could still serve to resolve DNA entanglements or promote chromosome organization and segregation without generating detectable haplotype reshuffling.

Deletion of *DMC1* or *SPO11* in the heterozygous BH background produced a striking reduction in viable progeny from dissected titan cells, and whole-genome sequencing of the survivors revealed widespread LOH and aneuploidy, often at a whole-chromosome scale and linked with smaller colony size. This result suggests that Dmc1 and Spo11 may act to stabilize chromosome segregation during depolyploidization, and that their loss converts the reduction division into an error-prone process that yields uniparental disomy (LOH) and copy number imbalance. Mechanistically, segregation defects can arise from multiple, non-exclusive failures: erroneous kinetochore–microtubule attachments (38, 39), sister-chromatid cohesion defects (40, 41), abnormal centrosome or centriole numbers (42-44), or an impaired spindle assembly checkpoint (SAC) (45-47). Any of these will increase non-disjunction and thereby contribute to the LOH or aneuploidy we observed. The stronger defect in BH *dmc1*Δ/*dmc1*Δ suggests that Dmc1-mediated homology tethering may be especially important to align homologous chromosomes and suppress merotelic attachment. Distinguishing among these possibilities will require further investigation involving live imaging of centromere-tagged chromosomes during titan depolyploidization, quantitative assays of kinetochore occupancy and error correction, cohesion localization, spindle-pole body counting, or dynamics in function of key components of SAC (Mad1, Mad2, or Bub1) in wild type versus *dmc1* and *spo11* deletion mutants.

Based on our observations in this study, when titan cells were induced from a haploid parent (H99), all titan-derived colonies had a haploid DNA content, whereas titan cells induced

from diploid parents (CnLC6683 or BH) produced colonies that predominantly have a diploid DNA content. This concordance between the parental ploidy and the major ploidy of progeny implies that the ploidy reduction process proceeds under tight control to restore a balanced genome. Here, we envision a multi-stage process: host-like and environmental cues (nutrient limitation, low pH, CO_2, serum components, low cell density (13-15, 48, 49)) trigger the highly regulated process of titanization and endoreplication (16, 48, 50), yielding a uninucleate but highly polyploid cell with altered wall and capsule architecture and stress tolerance (7, 11, 18, 51). During the subsequent reduction phase, titan cells may execute a replication-licensed step analogous to a pre-reduction S-phase, reorganize their spindles, and engage meiotic toolkit components (including Dmc1 and Spo11) to promote homolog engagement and faithful segregation without invoking frequent canonical crossovers. Once the segregation "state" is established, daughter cells emerge by budding. This is consistent with our observation that when we dissected daughter cells budding from titan cells, while in most cases only one daughter cell was produced at a time, there were also occasions where two daughter cells were produced simultaneously at different locations of the titan cell. In addition, the budding process usually occurs after a noticeable lag before the first daughter cell is produced, with subsequent budding events occurring with shorter intervals. We hypothesize that the DNA content for daughter cells might be prepared and packed together inside the titan cell before the budding process starts. Thus, titan cells could also serve as storages sites for genetic information under stressful and challenging conditions, allowing daughter cells to be quickly produced to repopulate the niche when favorable conditions return, which requires meiosis-specific genes (e.g. *DMC1* and *SPO11*) to ensure faithful return to the original parental ploidy.

Figure legends

Figure 1. Investigating the role of *DMC1* and *SPO11* during ploidy reduction in different genetic backgrounds.

(A) Pre- and post-filtration titan cell cultures were imaged by light microscopy, and then used for cell diameter measurement. Cells collected from each culture were analyzed by flow cytometry. Filtered titan cell population has increased proportion of larger polyploid cells. **(B)** Ploidy levels of the progenitor strains are inherited in the produced daughter cells after titanization. **(C-E)** Percentage of dissected titan or yeast-like cells that can form colonies was assessed in the BH (C), H99 (D) and CnLC6683 (E) background.

Figure 2. Titan colony cells derived from mutant BH strains have diverse carbon source utilization profiles.

(A) 12 titan colony cells from each the BH, BH *dmc1*Δ/*dmc1*Δ and BH *spo11*Δ/*spo11*Δ mutant strains were used for carbon sources utilization assay. Cell growth in carbon sources including D-ribose, L-arabinose, maltose, and sucrose were calculated using optical density measured 6-dpi with normalization against their growth in glucose. The assay was repeated twice and data from both were plotted. The difference in variation among titan colony cells derived from different genotypes was assessed by Levene's test (**, $P < 0.01$; *, $P < 0.1$). **(B)** The same assay was performed for CnLC6683, CnLC6683 *dmc1*Δ/*dmc1*Δ, and CnLC6683 *spo11*Δ/*spo11*Δ mutants. In contrast to the BH background, for majority tested group of cells, Levene's test showed no significant difference in variation among titan colony cells derived from the three genotypes under CnLC6683 background.

Figure 3. *DMC1* and *SPO11* are critical for chromosome stability during the ploidy reduction of titan cells with heterozygous genomes.

(A) A variety of LOH and aneuploid events were identified in titan colony cells derived from BH *dmc1*Δ/*dmc1*Δ and BH *spo11*Δ/*spo11*Δ mutants, which were categorized into six types. (B) Number of events identified for each of the six types. *: Number of cells with haploid or triploid DNA content based on flow cytometry analysis. (C) Percentage of dissected titan cells that failed to form a colony or formed a colony cell with normal or abnormal (contain events belonging to

any of the six types) genome content. (D) Dissected titan cells can form both large and small colonies, marked with green and yellow arrows, respectively.

Figure 4. No canonical meiotic recombination was detected in BH titan daughter cells. **(A)** Titan daughter cells were used for recombination analysis and lineage dissection of BH titan cell 4 is shown as an example. **(B)** LOH events identified in cells dissected in group 6 using whole-genome sequencing data. **(C)** Pipeline of recombination analysis in heterozygous diploid using nanopore sequencing results. **(D)** Output of the nanopore read analysis pipeline of 10 progeny samples in green compared to simulated samples with and without artificial crossover events in red. Counts of potentially chimeric reads containing breakpoints within 10kb windows were normalized to the genome-wide read depth for each sample.

Supplemental figure legends

Supplemental Figure S1. Pilot assay of carbon source utilization of titan colony cells using Biolog YT microplates.

Metabolite oxidation and assimilate utilization by tested titan colony cells were plotted. Principle component analysis was performed to determine which carbon sources contributed greatest to variance between tested lines. Total loadings for the first two principle components then were used to select carbon sources where variation between lines was likely to be observed. D-ribose, L-arabinose, maltose, and sucrose were selected for the following assays in expanded sets of titan colony cells.

Supplemental Figure S2. Levene's test of difference in variation among titan colony cells.

Variance in the growth after 6 days for progeny of *dmc1*Δ/*dmc1*Δ, *spo11*Δ/*spo11*Δ mutants, and wild-type BH (A) and CnLC6683 (B) were compared with Levene's test for equal variances. The mean value of each titan colony cell's growth in a carbon substrate was normalized by dividing by the mean growth in D-glucose for that titan colony cell. The variance of these normalized means were then compared, with the difference in variance and significance of the test statistic plotted for each genotype and carbon source, from two experimental repeats.

Supplemental Figure S3. Flow cytometry analysis of titan colony cells.

Flow cytometry analysis results of titan colony cells with haploid- or triploid-like DNA content.

Supplemental Figure S4. Lineage dissection of BH titan cells.

(A) Lineage dissection maps of 9 BH titan cells that produced daughter cells. **(B)** Cells in group 6 all formed small size colonies compared to wild-type BH on YPD agar media.

Supplemental Figure S5. Developed program can identify recombination and partial chromosome LOH event in heterozygous diploid background.

Reads plots showing breakpoints representing recombination (left) and LOH (right) events identified in simulated sample using developed program.

MATERIALS AND METHODS

Strains, media and growth conditions

C. neoformans strains used in this study are listed in Supplemental Table 1. Fresh cultures were revived and maintained on YPD (1% yeast extract, 2% Bacto Peptone, 2% dextrose) agar media, supplemented with appropriate antifungal drugs (nourseothricin (NAT) at 100 μg/mL or neomycin (G418) at 200 μg/mL) when needed, and incubated at 30°C. Titan cell induction was performed using the published methods from Ballou's lab (7). Briefly, cells were incubated in Yeast Nitrogen Base (YNB) liquid media with 2% glucose at 30˚C overnight, followed by adjusting OD to 0.001 and incubated in PBS with 10% Fetal Bovine Serum (FCS) (Thermo Fisher, USA) at 37˚C with 5% CO2. Cell cultures were then washed with PBS for 3 times, centrifuged, and resuspended in PBS. Titan cell and titan daughter cell dissection was carried out using a Nikon yeast spore dissection microscope equipped with a glass fiber needle 25 μm in diameter.

Construction of mutant strains

Deletion mutant strains were generated in the *C. neoformans* H99, Bt63, or CnLC6683 backgrounds. To generate the deletion alleles, the *NAT* or *NEO* gene expression cassette was amplified from plasmids pAI3 and pJAF1, respectively. Approximately 1.5-kb regions (homologous arms) flanking the genes of interest were amplified from wild-type strain genomic DNA and fused with the *NAT* or *NEO* drug resistance marker with overlapping PCR, as previously described (52), to generate the donor DNA cassettes. CRISPR-Cas9-directed mutagenesis was used for mutant generation. The CAS9 cassette was PCR-amplified from plasmid pXL-1 with universal primers M13F and M13R (52). The desired target sequences for the sgRNA constructs were designed using the Eukaryotic Pathogen CRISPR guide RNA/DNA Design Tool (EuPaGDT) with default parameters (53). Two gRNAs were designed and used for each gene of interest. Complete gRNAs were generated by one-step overlap PCR. About 1.5 μg donor DNA cassette, 400 ng CAS9 cassette, and 150 ng of each complete gRNAs fragment were mixed and condensed to a 5 μL volume before being introduced to strains with the transient CRISPR/Cas9 coupled with electroporation (TRACE) transformation approach (52). The obtained transformants were validated by genotyping using diagnostic PCRs for the internal

region of the ORF, 5'-junction and 3'-junction regions, as well as spanning PCR of the region encompassing the deletion construct as previously described (54).

Generation of BH *dmc1*Δ/*dmc1*Δ and BH *spo11*Δ/*spo11*Δ mutant strain

To generate the heterozygous diploid strain BH, the H99α mutant *ura5*::*NEO* and wild-type Bt63**a** cells were mixed in equal proportions in ddH_2O and inoculated and incubated on V8 medium for 48 hours at room temperature in the dark to allow cell fusion. The cells were then harvested and plated on YPD + NEO solid medium plates to isolate single colonies, with 150-200 colonies per plate. Colonies from YPD + NEO plate were replica-plated onto SD-uracil agar medium (0.67% nitrogen base w/o amino acid, 0.002% uracil drop out mix, 2% agar, 2% dextrose) and incubated at 30°C. Colonies that could grow on both YPD + NEO and SD-uracil agar plates were recovered on YPD + NEO and maintained as yeast colonies. Colony PCR was performed to confirm the presence of both the **a** and the α mating types. Flow cytometry and whole genome sequencing were used to confirm the ploidy of the resulting diploid strain BH.

Flow cytometry analysis

Samples for flow cytometry analysis to determine *Cryptococcus* ploidy was prepared as previously described (58, 63). The Flow cytometry analysis was performed at the Duke Cancer Institute Flow Cytometry Shared Resource Laboratory (33, 55).

Carbon source utilization assay and statistical analysis

To assess metabolic traits which varied among titan colony cells, Biolog YT Microplates (Biolog, Inc., Hayward, CA, USA) were inoculated in triplicate, using BUY agar, YT inoculating solution, and the suggested optical density, then incubated at 28°C in a humid enclosure. Data were collected at 3 days post inoculation, when absorbance was read at 500 nm for oxidation tests and 590 nm for assimilation tests. Values in each plate were blanked based on the absorbance of the negative control and divided by the growth in D-glucose for normalization. Principle component analysis (PCA) was performed on the normalized values, then the loadings were determined to identify the amount of variance explained by each carbon source in the overall matrix. Carbon sources that explained high amounts of the variance for both were used for testing a smaller number of carbon sources with additional titan colony cells.

Variability of titan colony cell growth was then evaluated via assimilation of selected carbon sources. D-ribose, L-arabinose, maltose, and sucrose were selected as carbon sources, with D-glucose as a control treatment for normalization. Twelve titan colony cells of each genotype were grown in triplicate in 96 well microtiter plates (Falcon, USA) in 160 µl YNB supplemented with 666 mM per C atom of each carbon source (i.e. 111 mM for D-glucose, 133 mM for D-ribose) for up to 6 days at 28°C, with daily measurements of absorbance at 600 nm. For comparison of variance among progeny, absorbance values were log-transformed, then averaged by strain and normalized to the D-glucose condition. Mean normalized absorbances of each genotype were then used to compared variances of mutant titan colony cells to the variance of wild-type titan colony cells with Levene's test.

Whole genome sequencing and nanopore sequencing

DNA for genotyping and Illumina whole genome sequencing were prepared as previously described (33). Illumina sequencing was conducted at the Duke Sequencing and Genomic Technologies core facility (https://genome.duke.edu), on a Novaseq 6000 platform with 250 bp paired-end option. High molecular weight genomic DNA samples for Nanopore long read sequencing were prepared using a modified CTAB protocol as previously described (20). Nanopore long-read sequencing was conducted in house using a MinION device with R10.4.1 flow cells following instructions provided by the manufacturer. All of the sequencing data have been deposited in the BioProject ID PRJNA1328773.

Read depth analysis of short-read sequencing data

Illumina short read sequences for all samples were analyzed using WeavePop (v1.0.0) (56). Sequences were aligned to a combined H99 and Bt63 reference genome and copy number variants were called from the resulting read depth.

Recombination detection using Nanopore long reads

Long Nanopore reads from progeny samples were aligned to reference genomes using the lra aligner (v1.3.7) (57), with separate alignments performed against the H99 major parental reference, the Bt63 minor parental reference, and a concatenated reference containing both genomes. Alignment files were processed using samtools (v1.18) (58) for sorting, indexing, and

extracting unmapped reads. Bedtools (v2.31.0) (59) was used to convert BAM files to BED format for downstream analysis. Reference genomes were preprocessed to ensure consistent chromosome naming and ordering. Whole-genome alignments between parental references were generated with wfmash (v0.10.) (60) and structural variant detection was performed with SyRI (v1.6.3) (61) to identify SNPs, insertions, and deletions distinguishing the parental haplotypes.

Following alignment, known SNPs and indels distinguishing the H99 and Bt63 parental genomes were identified from syri output and filtered to retain only SNPs. The resulting file was analyzed using a pipeline implemented in python (v3.7.12). Using pybedtools (v0.9.0) (62) and pandas (v1.3.5) (63), intersections between aligned reads and SNP positions were computed for each chromosome. For each read overlapping a SNP, the base was compared to both parental references and assigned to H99, Bt63, or marked as unknown. This parent-calling step was parallelized by chromosome using Python's multiprocess (v0.70.14) (64) and pysam (v0.21.0) libraries.

Consecutive SNPs with identical parent assignments were merged into stretches, and short stretches less than 1000bp and containing fewer than 4 SNPs were merged into the subsequent stretch to reduce the impact of sequencing errors. Reads containing substantial stretches that were assigned to both parents were flagged as chimeric. Breakpoint positions where parent assignment switched were extracted and their frequency across the genome was calculated. Data visualization and further analysis were performed using matplotlib (v3.5.3) (65), seaborn (v0.12.2) (66), and numpy (v1.21.6) (67), with candidate chimeric reads and breakpoint loci summarized in output tables and plots.

Wild-type progeny comparison with simulated long reads

Simulated long-read datasets were generated with PBSIM3 (v3.0.0) (68), which sampled progeny Nanopore reads to match the error profile and length distribution observed in the data. Recombinant and non-recombinant genomes were constructed by swapping defined regions of random chromosomes between parental references, and concatenated FASTA files were used as templates for simulation. PBSIM3 was run in whole-genome sampling mode with a target depth of 20×, producing simulated FASTQ files for both recombinant and unrecombined genomes.

To account for differences in sequencing depth across samples, the number of chimeric reads at each breakpoint position was normalized by dividing by the average genome-wide read

depth for each sample. Average depth was calculated from coverage statistics generated by samtools, and normalization was performed prior to plotting. Breakpoint densities for simulated samples and 10 wild type experimental samples were visualized together with seaborn and matplotlib. For each chromosome, breakpoint positions were binned and plotted as normalized histograms, with each sample assigned a distinct color and legend label. This allowed direct comparison of recombination signatures between simulated and experimental datasets, facilitating identification of regions with elevated chimeric read frequency. Regions with a normalized breakpoint frequency greater than 0.5 were selected and the pileup of reads underlying the loci were inspected for signatures of canonical recombination. A crossover signal was defined as a locus where more than 60% of the reads supported a switching between parental haplotypes at the breakpoint location, and two types of reciprocal chimeric reads were present in approximately equal frequencies. A loss of heterozygosity signal was defined as a locus where more than 20% of the reads supported a switching between parental haplotypes at the breakpoint location, and only one type of chimeric read was present.

Acknowledgments

This work was supported by NIH/NIAID awards R01AI050113-20, R01AI039115-28, R01AI133654-08 to JH. JH is a fellow and co-director with Leah Cowen of the CIFAR program Fungal Kingdom: Threats & Opportunities.

Statement of competing interest

The authors declare no competing interests.

REFERENCES

1. C. C. Chang *et al.*, Global guideline for the diagnosis and management of cryptococcosis: an initiative of the ECMM and ISHAM in cooperation with the ASM. *Lancet. Infect. Dis.* **24**, e495-e512 (2024).
2. Y. Bahn, S. Sun, J. Heitman, X. Lin, Microbe profile: *Cryptococcus neoformans* species complex. *Microbiol.* **166**, 797-799 (2020).
3. R. Rajasingham *et al.*, The global burden of HIV-associated cryptococcal infection in adults in 2020: a modelling analysis. *Lancet Infect. Dis.* **22**, 1748-1755 (2022).
4. J. W. Kronstad *et al.*, Expanding fungal pathogenesis: *Cryptococcus* breaks out of the opportunistic box. *Nat. Rev. Microbiol.* **9**, 193-203 (2011).
5. S. T. Denham *et al.*, A dissemination-prone morphotype enhances extrapulmonary organ entry by *Cryptococcus neoformans*. *Cell Host Microbe* **30**, 1382-1400 e1388 (2022).
6. J. G. Cruickshank, R. Cavill, M. Jelbert, *Cryptococcus neoformans* of unusual morphology. *Appl. Microbiol.* **25**, 309-312 (1973).
7. I. M. Dambuza *et al.*, The *Cryptococcus neoformans* Titan cell is an inducible and regulated morphotype underlying pathogenesis. *PLOS Pathogens* **14**, e1006978 (2018).
8. M. Feldmesser, Y. Kress, A. Casadevall, Dynamic changes in the morphology of *Cryptococcus neoformans* during murine pulmonary infection. *Microbiology* **147**, 2355-2365 (2001).
9. J. C. Brown, E. R. Ballou, Is *Cryptococcus neoformans* a pleomorphic fungus? *Curr. Opin. Microbiol.* **82**, 102539 (2024).
10. L. H. Okagaki, K. Nielsen, Titan cells confer protection from phagocytosis in *Cryptococcus neoformans* infections. *Eukaryot. cell* **11**, 820-826 (2012).
11. L. Mukaremera *et al.*, Titan cell production in *Cryptococcus neoformans* reshapes the cell wall and capsule composition during infection. *Cell Surf.* **1**, 15-24 (2018).
12. M. Probert *et al.*, A glucuronoxylomannan epitope exhibits serotype-specific accessibility and redistributes towards the capsule surface during titanization of the fungal pathogen *Cryptococcus neoformans*. *Infect. Immun.* **87**, 10.1128/iai. 00731-00718 (2019).
13. O. Zaragoza *et al.*, Fungal cell gigantism during mammalian infection. *PLOS Pathogens* **6**, e1000945 (2010).
14. L. H. Okagaki *et al.*, Cryptococcal cell morphology affects host cell interactions and pathogenicity. *PLOS Pathogens* **6**, 15 (2010).
15. N. Trevijano-Contador *et al.*, *Cryptococcus neoformans* can form titan-like cells in vitro in response to multiple signals. *PLOS Pathogens* **14**, e1007007 (2018).
16. L. Saidykhan *et al.*, An in vitro method for inducing titan cells reveals novel features of yeast-to-titan switching in the human fungal pathogen *Cryptococcus gattii*. *PLOS Pathogens* **18**, e1010321 (2022).
17. B. Hommel *et al.*, Titan cells formation in *Cryptococcus neoformans* is finely tuned by environmental conditions and modulated by positive and negative genetic regulators. *PLOS Pathogens* **14**, e1006982 (2018).
18. A. C. Gerstein *et al.*, Polyploid titan cells produce haploid and aneuploid progeny to promote stress adaptation. *mBio* **6**, e01340-01315 (2015).
19. Y. Zhao, Y. Wang, S. Upadhyay, C. Xue, X. Lin, Activation of meiotic genes mediates ploidy reduction during *Cryptococcal* infection. *Curr. Biol.* **30**, 1387-1396 e1385 (2020).
20. V. Yadav, S. Sun, J. Heitman, Uniparental nuclear inheritance following bisexual mating in fungi. *eLife* **10**, e66234 (2021).

21. X. Lin, C. M. Hull, J. Heitman, Sexual reproduction between partners of the same mating type in *Cryptococcus neoformans*. *Nature* **434**, 1017-1021 (2005).
22. K. J. Kwon-Chung, A new genus, *Filobasidiella*, the perfect state of *Cryptococcus neoformans*. *Mycologia* **67**, 1197-1200 (1975).
23. K. J. Kwon-Chung, Morphogenesis of *Filobasidiella neoformans*, the sexual state of *Cryptococcus neoformans*. *Mycologia* **68**, 821-833 (1976).
24. K. J. Kwon-Chung, A new species of *Filobasidiella*, the sexual state of *Cryptococcus neoformans* B and C serotypes. *Mycologia* **68**, 942-946 (1976).
25. I. Lam, S. Keeney, Mechanism and regulation of meiotic recombination initiation. *Cold Spring Harbor perspect. Biol.* **7**, a016634 (2015).
26. D. K. Bishop, D. Park, L. Xu, N. Kleckner, *DMC1*: a meiosis-specific yeast homolog of E. coli recA required for recombination, synaptonemal complex formation, and cell cycle progression. *Cell* **69**, 439-456 (1992).
27. W. R. Rice, A. K. Chippindale, Sexual recombination and the power of natural selection. *Science* **294**, 555-559 (2001).
28. S. C. Ortiz, C. M. Hull, Biogenesis, germination, and pathogenesis of *Cryptococcus* spores. *Microbiol. Mol. Biol. Rev.* **88**, e00196-00123 (2024).
29. F. Ianzini *et al.*, Activation of meiosis-specific genes is associated with depolyploidization of human tumor cells following radiation-induced mitotic catastrophe. *Cancer Res.* **69**, 2296-2304 (2009).
30. X. F. Wang *et al.*, Polyploid mitosis and depolyploidization promote chromosomal instability and tumor progression in a Notch-induced tumor model. *Dev. Cell* **56**, 1976-1988 e1974 (2021).
31. M. Z. Anderson, G. J. Thomson, M. P. Hirakawa, R. J. Bennett, A ‘parameiosis’ drives depolyploidization and homologous recombination in *Candida albicans*. *Nat. Commun.* **10**, 4388 (2019).
32. A. Forche *et al.*, The parasexual cycle in *Candida albicans* provides an alternative pathway to meiosis for the formation of recombinant strains. *PLOS Biol.* **6**, e110 (2008).
33. P. P. Peterson *et al.*, The *Cryptococcus neoformans* STRIPAK complex controls genome stability, sexual development, and virulence. *PLOS Pathogens* **20**, e1012735 (2024).
34. G. Janbon *et al.*, Analysis of the genome and transcriptome of *Cryptococcus neoformans* var. grubii reveals complex RNA expression and microevolution leading to virulence attenuation. *PLOS Genetics* **10**, e1004261 (2014).
35. M. S. McMahill, C. W. Sham, D. K. Bishop, Synthesis-dependent strand annealing in meiosis. *PLOS Biol.* **5**, e299 (2007).
36. F. Pâques, J. E. Haber, Multiple pathways of recombination induced by double-strand breaks in *Saccharomyces cerevisiae*. *Microbiol. Mol. Biol. Rev.* **63**, 349-404 (1999).
37. A. L. Williams *et al.*, Non-crossover gene conversions show strong GC bias and unexpected clustering in humans. *eLife* **4**, e04637 (2015).
38. S. F. Bakhoum, G. Genovese, D. A. Compton, Deviant kinetochore microtubule dynamics underlie chromosomal instability. *Curr. Biol.* **19**, 1937-1942 (2009).
39. S. F. Bakhoum, S. L. Thompson, A. L. Manning, D. A. Compton, Genome stability is ensured by temporal control of kinetochore–microtubule dynamics. *Nat. Cell Biol.* **11**, 27-35 (2009).
40. M. Di Nardo, M. M. Pallotta, A. Musio, The multifaceted roles of cohesin in cancer. *J. Exp. Clin. Cancer Res.* **41**, 96 (2022).

41. D. Pati, Role of chromosomal cohesion and separation in aneuploidy and tumorigenesis. *Cell. Mol. Life Sci.* **81**, 100 (2024).
42. B. D. Vitre, D. W. Cleveland, Centrosomes, chromosome instability (CIN) and aneuploidy. *Curr. Opin. Cell Biol.* **24**, 809-815 (2012).
43. G. M. LoMastro, A. J. Holland, The emerging link between centrosome aberrations and metastasis. *Dev. cell* **49**, 325-331 (2019).
44. K. Yoshizawa, K. Yaguchi, R. Uehara, Uncoupling of DNA replication and centrosome duplication cycles is a primary cause of haploid instability in mammalian somatic cells. *Front. Cell Dev. Biol.* **8**, 721 (2020).
45. F. Foijer *et al.*, Chromosome instability induced by Mps1 and p53 mutation generates aggressive lymphomas exhibiting aneuploidy-induced stress. *Proc. Natl. Acad. Sci. USA* **111**, 13427-13432 (2014).
46. Y.-F. Gao *et al.*, Cdk1-phosphorylated CUEDC2 promotes spindle checkpoint inactivation and chromosomal instability. *Nat. Cell Biol.* **13**, 924-933 (2011).
47. H. Sapkota, E. Wasiak, J. R. Daum, G. J. Gorbsky, Multiple determinants and consequences of cohesion fatigue in mammalian cells. *Mol. Biol. Cell.* **29**, 1811-1824 (2018).
48. M. Caza, J. W. Kronstad, The cAMP/protein kinase a pathway regulates virulence and adaptation to host conditions in *Cryptococcus neoformans*. *Front. Cell. Infect. Microbiol.* **9**, 212 (2019).
49. T. R. O'Meara, S. M. Holmer, K. Selvig, F. Dietrich, A. J. Alspaugh, *Cryptococcus neoformans* Rim101 is associated with cell wall remodeling and evasion of the host immune responses. *mBio* **4**, 10.1128/mbio. 00522-00512 (2013).
50. L. H. Okagaki *et al.*, Cryptococcal titan cell formation is regulated by G-protein signaling in response to multiple stimuli. *Eukaryot. Cell* **10**, 1306-1316 (2011).
51. J. N. Crabtree *et al.*, Titan cell production enhances the virulence of *Cryptococcus neoformans*. *Infect. Immun.* **80**, 3776-3785 (2012).
52. Y. Fan, X. Lin, Multiple applications of a transient CRISPR-Cas9 coupled with electroporation (TRACE) system in the *Cryptococcus neoformans* species complex. *Genet.* **208**, 1357-1372 (2018).
53. D. Peng, R. Tarleton, EuPaGDT: a web tool tailored to design CRISPR guide RNAs for eukaryotic pathogens. *Microb. Genom.* **1**, e000033 (2015).
54. Z. Bian *et al.*, Essential genes encoded by the mating-type locus of the human fungal pathogen *Cryptococcus neoformans*. *mBio* **16**, e00223-00225 (2025).
55. R. Tanaka, H. Taguchi, K. Takeo, M. Miyaji, K. Nishimura, Determination of ploidy in *Cryptococcus neoformans* by flow cytometry. *J. Med. Vet. Mycol.* **34**, 299-301 (1996).
56. C. Zirión-Martínez, P. M. Magwene, WeavePop: A bioinformatics workflow to explore and analyze genomic variants of eukaryotic populations. *bioRxiv*, 2025.2008. 2015.670593 (2025).
57. J. Ren, M. J. P. Chaisson, lra: A long read aligner for sequences and contigs. *PLOS Comput. Biol.* **17**, e1009078 (2021).
58. H. Li *et al.*, The sequence alignment/map format and SAMtools. *Bioinformatics* **25**, 2078-2079 (2009).
59. A. R. Quinlan, I. M. Hall, BEDTools: a flexible suite of utilities for comparing genomic features. *Bioinformatics* **26**, 841-842 (2010).

60. A. Guarracino, N. Mwaniki, S. Marco-Sola, E. Garrison (2023) wfmash: whole-chromosome pairwise alignment using the hierarchical wavefront algorithm.
61. M. Goel, H. Sun, W.-B. Jiao, K. Schneeberger, SyRI: finding genomic rearrangements and local sequence differences from whole-genome assemblies. *Genome Biol.* **20**, 277 (2019).
62. R. K. Dale, B. S. Pedersen, A. R. Quinlan, Pybedtools: a flexible Python library for manipulating genomic datasets and annotations. *Bioinformatics* **27**, 3423-3424 (2011).
63. W. McKinney, Data structures for statistical computing in Python. *SciPy* **445**, 51-56 (2010).
64. M. M. McKerns, L. Strand, T. Sullivan, A. Fang, M. A. G. Aivazis, Building a framework for predictive science. *arXiv* 10.48550/arXiv.1202.1056 (2012).
65. J. D. Hunter, Matplotlib: A 2D graphics environment. *CiSE* **9**, 90-95 (2007).
66. M. L. Waskom, Seaborn: statistical data visualization. *JOSS* **6**, 3021 (2021).
67. C. R. Harris *et al.*, Array programming with NumPy. *Nature* **585**, 357-362 (2020).
68. Y. Ono, M. Hamada, K. Asai, PBSIM3: a simulator for all types of PacBio and ONT long reads. *NAR Genom. Bioinform.* **4**, lqac092 (2022).

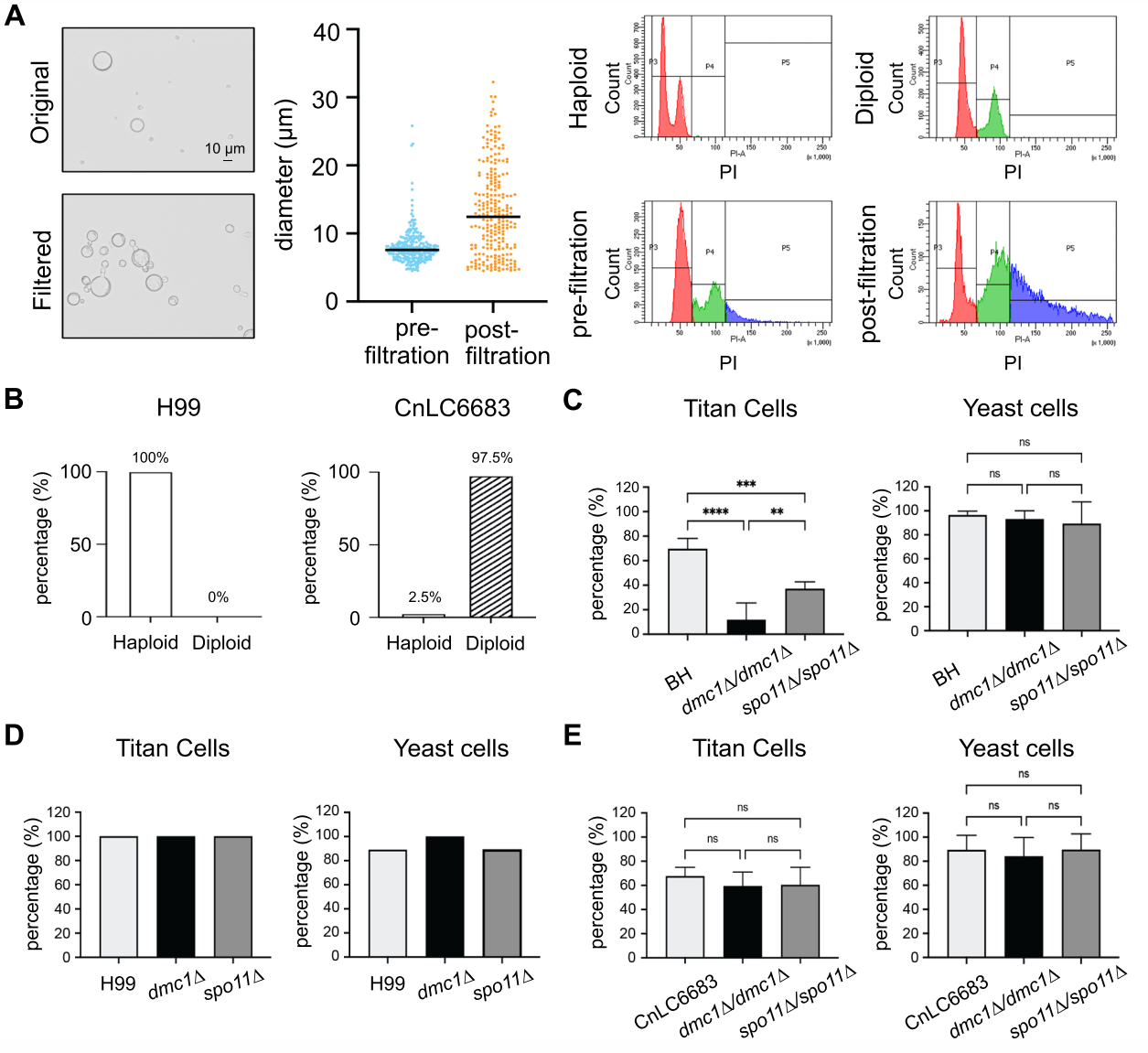
A
Original
Filtered
10 µm
diameter (µm)
40
30
20
10
0
pre-filtration
post-filtration
Haploid
Diploid
pre-filtration
post-filtration
Count
PI
P3
P4
P5
B
H99
CnLC6683
percentage (%)
100%
0%
97.5%
2.5%
Haploid
Diploid
C
Titan Cells
Yeast cells
***
****
**
ns
BH
dmc1Δ/dmc1Δ
spo11Δ/spo11Δ
D
Titan Cells
Yeast cells
H99
dmc1Δ
spo11Δ
E
Titan Cells
Yeast cells
CnLC6683
dmc1Δ/dmc1Δ
spo11Δ/spo11Δ

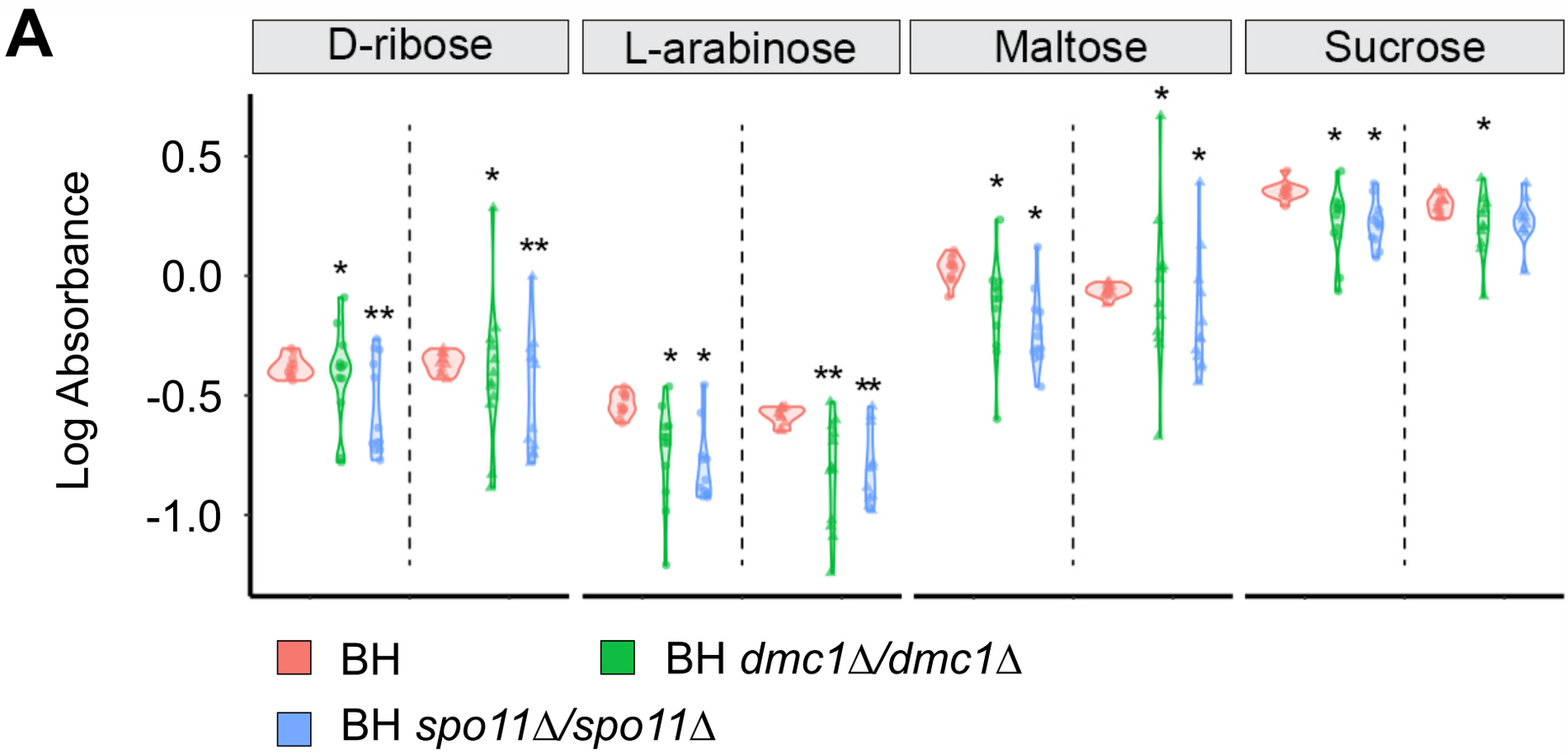
A
D-ribose
L-arabinose
Maltose
Sucrose
Log Absorbance
0.5
0.0
-0.5
-1.0
BH
BH dmc1Δ/dmc1Δ
BH spo11Δ/spo11Δ

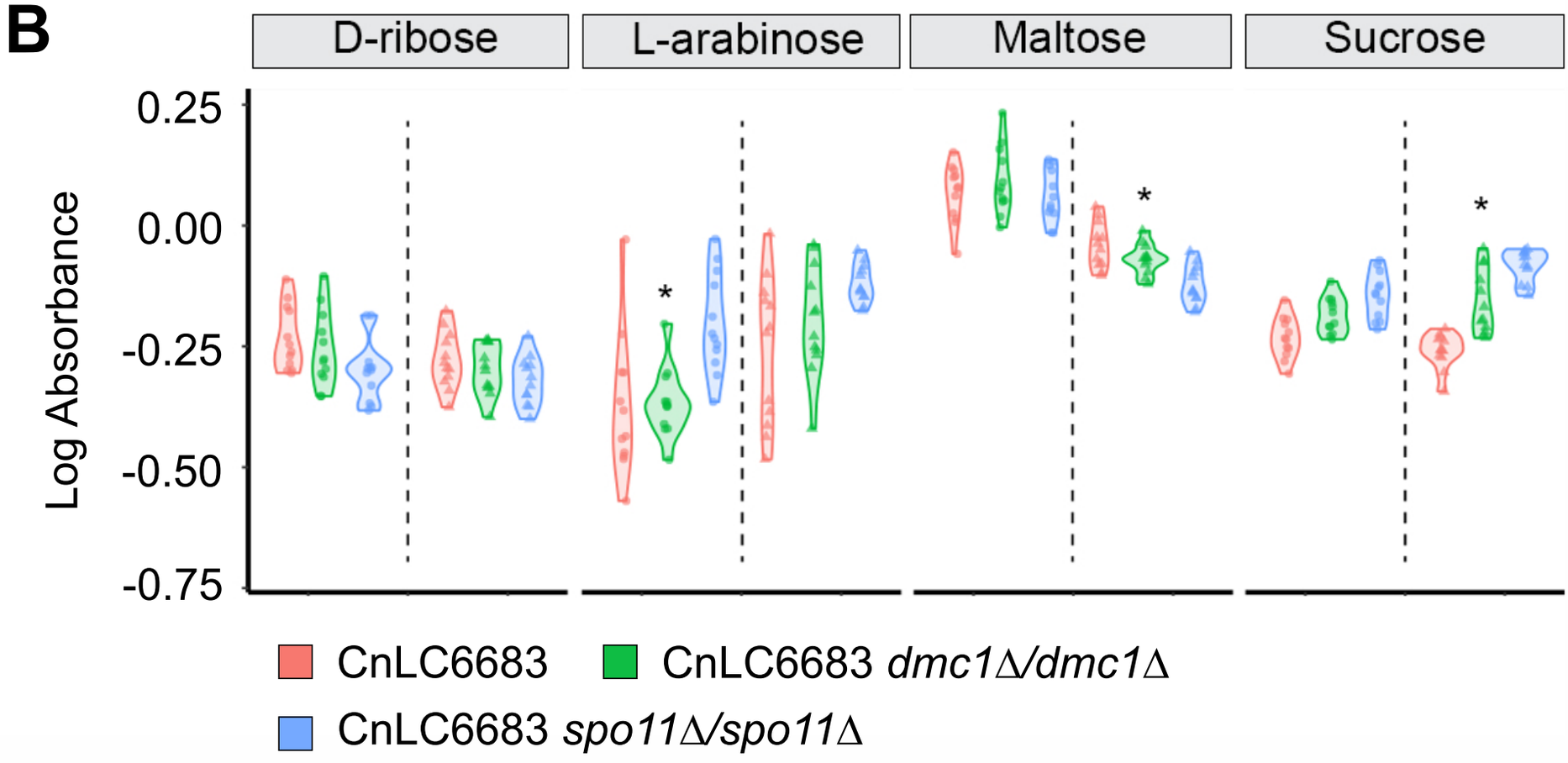
B
D-ribose
L-arabinose
Maltose
Sucrose
Log Absorbance
0.25
0.00
-0.25
-0.50
-0.75
CnLC6683
CnLC6683 dmc1Δ/dmc1Δ
CnLC6683 spo11Δ/spo11Δ

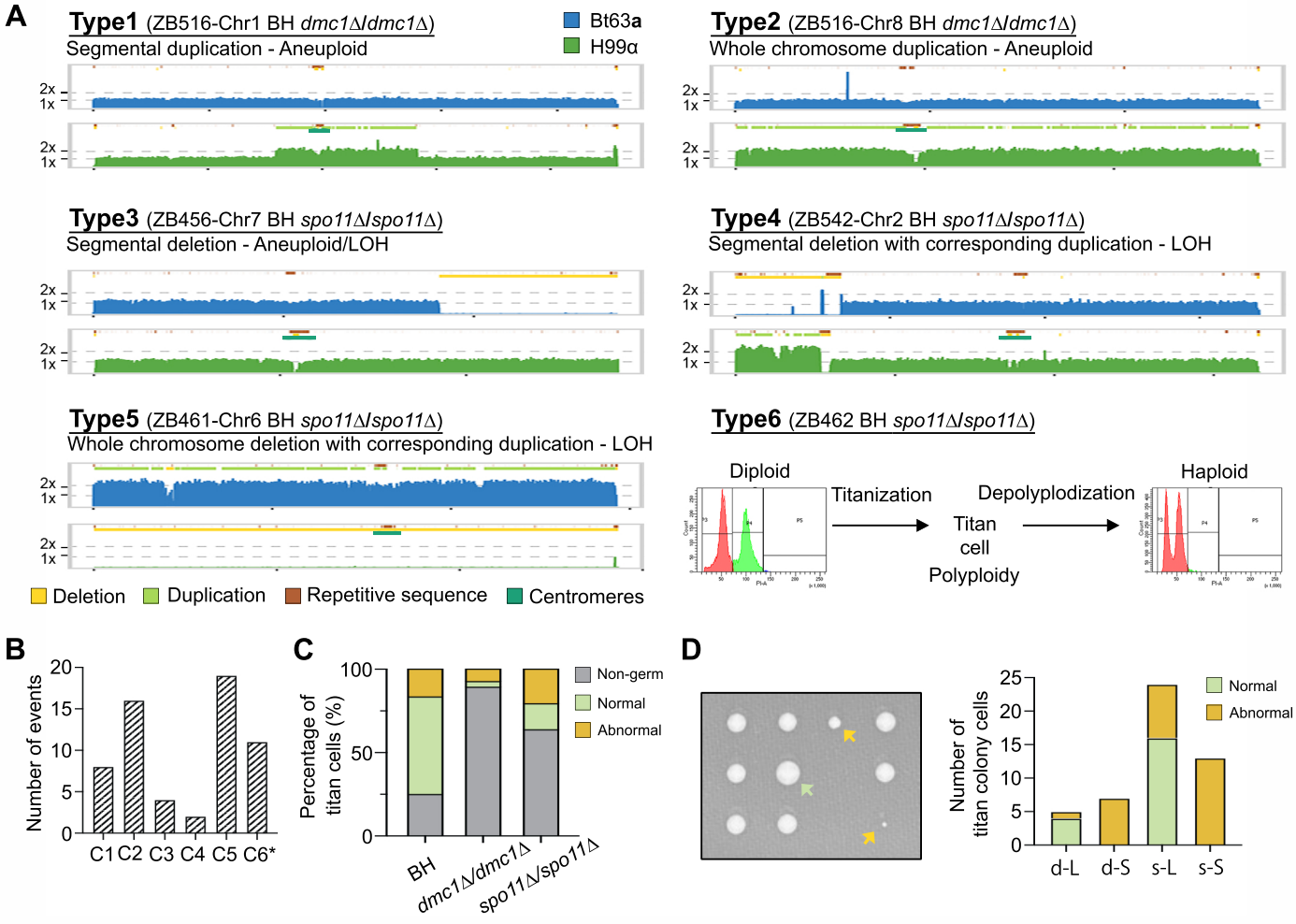
A
Type1 (ZB516-Chr1 BH dmc1Δ/dmc1Δ)
Segmental duplication - Aneuploid
Bt63a
H99α
Type2 (ZB516-Chr8 BH dmc1Δ/dmc1Δ)
Whole chromosome duplication - Aneuploid
Type3 (ZB456-Chr7 BH spo11Δ/spo11Δ)
Segmental deletion - Aneuploid/LOH
Type4 (ZB542-Chr2 BH spo11Δ/spo11Δ)
Segmental deletion with corresponding duplication - LOH
Type5 (ZB461-Chr6 BH spo11Δ/spo11Δ)
Whole chromosome deletion with corresponding duplication - LOH
Type6 (ZB462 BH spo11Δ/spo11Δ)
Diploid
Titanization
Titan cell
Polyploidy
Depolyplodization
Haploid
2x
1x
Deletion
Duplication
Repetitive sequence
Centromeres
B
Number of events
C1 C2 C3 C4 C5 C6*
C
Percentage of titan cells (%)
Non-germ
Normal
Abnormal
BH
dmc1Δ/dmc1Δ
spo11Δ/spo11Δ
D
Number of titan colony cells
Normal
Abnormal
d-L
d-S
s-L
s-S

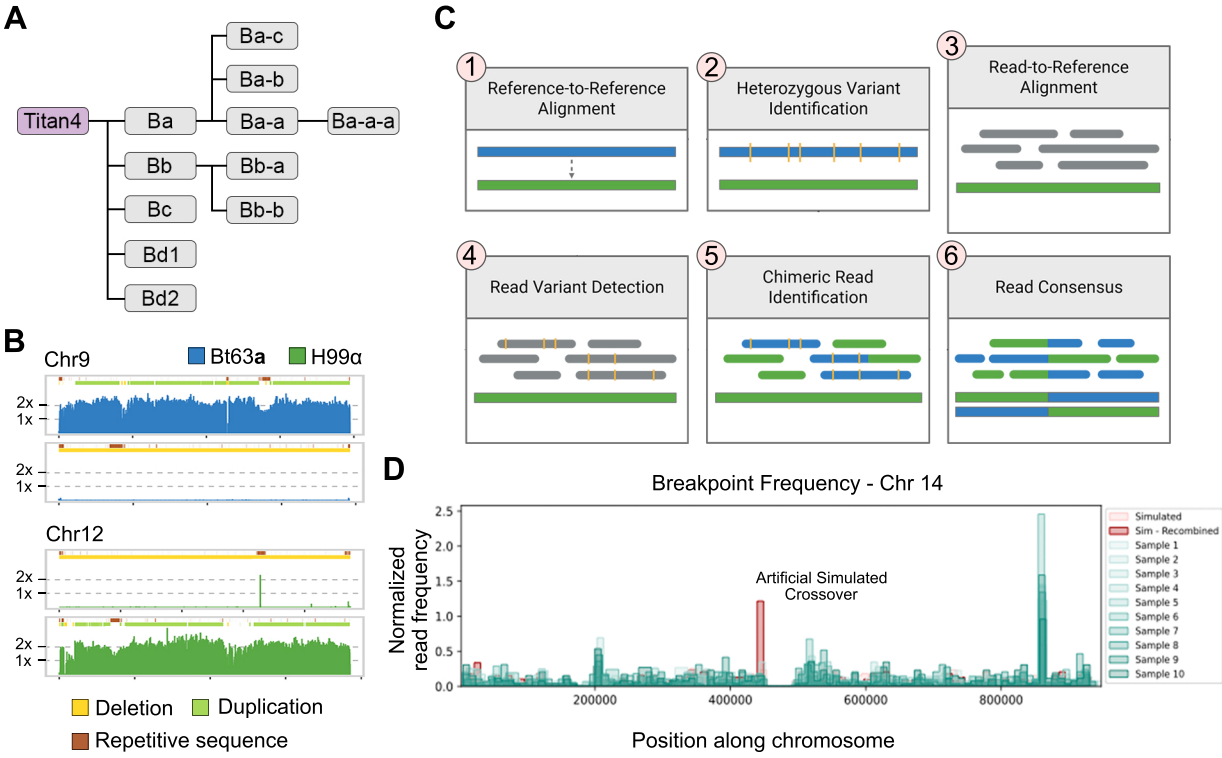
A
Titan4
Ba
Bb
Bc
Bd1
Bd2
Ba-c
Ba-b
Ba-a
Ba-a-a
Bb-a
Bb-b
B
Chr9
Bt63a
H99α
2x
1x
Chr12
Deletion
Duplication
Repetitive sequence
C
1 Reference-to-Reference Alignment
2 Heterozygous Variant Identification
3 Read-to-Reference Alignment
4 Read Variant Detection
5 Chimeric Read Identification
6 Read Consensus
D
Breakpoint Frequency - Chr 14
Normalized read frequency
Artificial Simulated Crossover
Position along chromosome
Simulated
Sim - Recombined
Sample 1
Sample 2
Sample 3
Sample 4
Sample 5
Sample 6
Sample 7
Sample 8
Sample 9
Sample 10